PHYSICAL REVIEW C VOLUME 45, NUMBER 4 APRIL 1992

Inelastic transverse electron scattering on ^{25}Mg

J. R. Marinelli
Departamento de Fisica da Universidade Federal de Santa Catarina, Florianópolis, Santa Catarina, Brazil

J. R. Moreira
Instituto de Fisica e Instituto de Eletrotécnica e Energia da Universidade de São Paulo, São Paulo, Brazil

(Received 4 October 1990)

Measurements of inelastic electron cross sections from ^{25}Mg at a backward angle and in the energy range 120 to 260 MeV are analyzed, and transverse form-factors results for the two lowest excited levels of the fundamental band were extracted. This new information is compared with rotational model calculations, in which the collective current contributions are included in phenomenological ways and on more microscopic theoretical grounds. For the energy levels considered the overall agreement is good, although no clear distinction between the various approximations for the rotational current could be made with the presently available data.

PACS number(s): 25.30.Dh, 21.60.Ev, 27.30.+t

I. INTRODUCTION

It is well known that the ground state ($\frac{5}{2}^+$) and states at 1.61 MeV ($\frac{7}{2}^+$) and 3.40 MeV ($\frac{9}{2}^+$) in ^{25}Mg can be classified as members of the ground-state rotational band. This interpretation is supported by several experimental results, including Coulomb form factors deduced from electron scattering [1,2]. Transverse form factors for elastic scattering on ^{25}Mg have already been calculated using three different models: projection on good angular momentum states [3], the particle-rotor model [4], and the shell model [5]. For the first two cases, the Nilsson model was used to describe the intrinsic structure. The results for these three models are numerically very much the same, yielding good agreement with available data. In particular, in the projection and particle-rotor models, it is apparent that important contributions to the form factors come from the core, especially for the $M1$ multipole, although most of the contribution is due to the unpaired nucleon in the field of the deformed potential. This fact appears as a general feature for deformed nuclei [3,6]. On the other hand, it is possible *a priori* to believe that collective contributions will be even more important for inelastic scattering in the fundamental band due to the presence of transverse electric multipoles, as will be discussed in the next sections.

Data from inelastic scattering on ^{25}Mg are available from experiments performed at the MIT-Bates electron accelerator and used to study only its ground state [7]. Reexamination of the information collected allowed us to extract new form-factor values in the incident electron energy range of 120–260 MeV and at a backward angle (160°). Knowing the inelastic Coulomb form factors obtained from other experiments, we were able to extract the corresponding transverse components. In this paper we analyze these new data and use, besides the projection and particle-rotor models, the cranking model for theoretical interpretation. The details of the experimental procedure, data analysis, and calculations are discussed in the following sections. Only the ^{25}Mg excited states cited above are considered here.

II. EXPERIMENTAL PROCEDURE AND DATA ANALYSIS

The data were extracted from an experiment carried out at the MIT Bates Linear Accelerator Center. A complete and detailed description of the high-resolution magnetic spectrometer and the electron detection system was already made [8,9]. A short presentation of the major parameters relevant to these data will be made here.

The electron incident beam energy was adjusted between 120 and 260 MeV. Incident current on the target was always lower than 10 μA. The targets used were ^{1}H in a polyethylene foil with a total thickness of 24.89 mg/cm^2 and Mg enriched up to 99.2% of ^{25}Mg with a thickness of 63.07 mg/cm^2. The other targets dimensions were 50 mm $\times$12.5 mm and 50 mm $\times$40 mm for H and Mg, respectively.

The analyzing spectrometer, set at 160°, was an energy-loss spectrometer [9]. Such a device allows the use of higher current intensity than a convention spectrometer, since the amount of heating on the target is distributed over a larger area and it is possible to use most of the exiting accelerator beam, and since a 1% energy spread on the incident beam still provides an energy resolution of 10^{-4} on the analyzed scattered electron spectra [10]. This is achieved with the proper design of the spectrometer, provided data collection is limited to electrons which have an energy-loss span lower than 1% [9], for which the spectrometer resolution reaches 2×10^{-4}. It is also possible to analyze a larger fraction of the emergent beam with a lower resolution. In our case this always happened, since the simultaneous observation of the elastic peak and inelastic levels up to 3.4 MeV is greater than the range for high-resolution spectrometer specification, even for the highest incident energy used (260 MeV).

Nevertheless, good spectra were obtained as shown in Fig. 1.

In this experiment the full angular aperture of the spectrometer was used with the horizontal slits set at $\theta_h = 26.18$ mrad and the vertical ones at $\theta_v = 152.40$ mrad. From the point of view of angular kinematical broadening, an energy resolution of $\Delta E/E < 10^{-4}$ is obtained for ^{25}Mg and of 6.6×10^{-4} for H [10]. Other effects such as kinematic broadening due to energy spread in the incident beam, finite target thickness, improper matching between incident beam geometric spread and spectrometer dispersion, spectrometer aberrations, and detector's finite resolution increase the expected experimental resolution. Nevertheless, since the data are corrected on line for some of these effects [10], the obtained experimental resolution is quite reasonable, as seen in Fig. 1.

The major scattered electron sensor is a multiple wire proportional counter (MWPC) with 99 cells, which detects electrons through an electrical discharge signal recorded by detectors assembled at two extreme ends of the sensor [8]. Identification of at least three cells and the three respective drift times is enough to position precisely the track of the scattered electron at the focal plane of the spectrometer [8].

The data were treated with various computer programs. For each particular energy level, several runs were performed with different physical positions of the MWPC in order to smooth, as much as possible, potential effects due to some particular channel inefficiency. These different runs were then added together, after performing corrections for the relative shift of the detector position.

To extract properly the relative cross sections from the experimental results, a line-shape calculation was performed according to Ref. [11]. With this technique we are considering Landau straggling, small-angle bremsstrahlung, and radiation emitted during large-angle scattering.

To take into account limitations of the linac-spectrometer combination, such as finite energy spread in the incident beam, finite beam spot size, detector dimensions, etc., which restrict the system resolution, the line shapes were folded with a Gaussian, whose half-width is defined by the shape of the elastic-scattering peak [12].

Once all these effects were incorporated in the line-shape curve, a χ^2 fitting with the experimental points was made adjusting amplitude and position of the curve. Figure 1 shows one particular spectrum with the best adjustment obtained. The reduced χ^2 is near 1 for the elastic and inelastic levels under examination. The quality of the fitting is similarly good for all other energies. Table I quotes the experimental cross-section values obtained for the two inelastic levels of interest and, for completeness, the elastic cross sections which were already analyzed in Ref. [7].

The extraction of the experimental transverse components was determined from the knowledge of the longitudinal form factors obtained from other experiments [1,13] at forward angles. A best-fit curve for these data

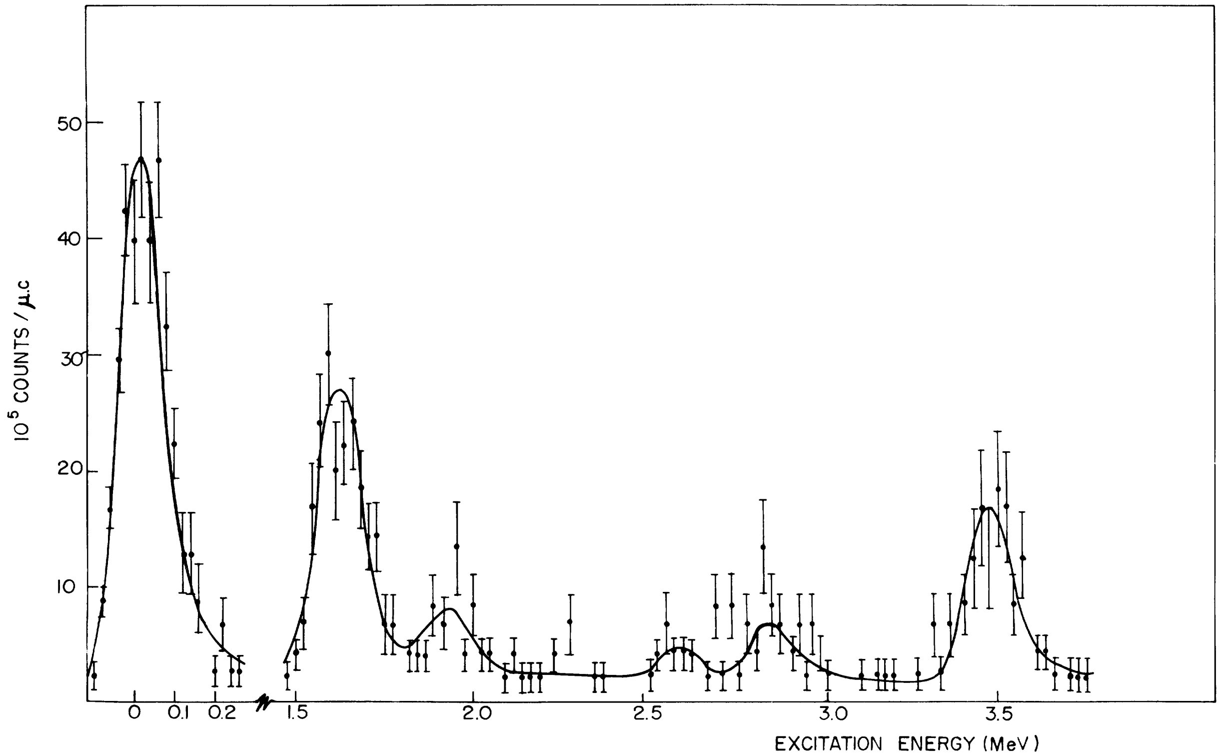

FIG. 1. Experimental spectrum for ^{25}Mg for 220 MeV incident electron energy. The solid curve corresponds to the best-fit line shape.

TABLE I. Experimental cross sections for ^{25}Mg, measured at $\theta = 160°$, for the various incident electron energies used in this experiment and the corresponding percentual errors.

	$d\sigma/d\Omega$ (fm^2/sr)			$\Delta\, d\sigma/d\Omega$ (%)		
E_i (MeV)	Elastic	1.612	3.405	Elastic	1.612	3.405
120.70	4.39×10^{-7}	3.71×10^{-7}	1.73×10^{-7}	7.7	7.6	9.8
140.44	1.37×10^{-7}	9.10×10^{-8}	5.11×10^{-8}	8.0	9.0	11.9
157.39	1.14×10^{-7}	2.25×10^{-8}	2.26×10^{-8}	6.1	10.2	10.2
160.21	1.17×10^{-7}	2.19×10^{-8}	2.28×10^{-8}	6.8	13.7	13.6
170.11	1.01×10^{-7}	1.89×10^{-8}	1.65×10^{-8}	6.9	13.2	14.5
179.01	7.17×10^{-8}	1.11×10^{-8}	1.24×10^{-8}	6.8	13.5	13.7
199.79	2.84×10^{-8}	1.11×10^{-8}	8.75×10^{-9}	8.1	10.8	12.3
220.41	1.26×10^{-8}	6.82×10^{-9}	3.38×10^{-9}	11.1	13.6	20.7
259.33	3.00×10^{-9}	1.84×10^{-9}	8.25×10^{-10}	11.0	13.0	21.3

was constructed using a phenomenological Fermi three-parameter charge distribution and the Tassie model, with the help of a distorted-wave Born approximation (DWBA) code. The transition charge distributions so obtained are used to calculate the longitudinal form factors at the conditions of the experiment. These form factors were then subtracted from the total ones using the well-known plane-wave Born approximation (PWBA) expression. The uncertainties inherent in this procedure are greatly minimized in the energy range between 160 and 200 MeV by the clear dominance of the transverse components. At smaller or higher beam energies, larger uncertainties can be seen in the final results shown in Sec. IV due to the smaller transverse and relatively larger longitudinal components.

III. THEORETICAL BACKGROUND

In the present work, the main results of Ref. [6] were used to calculate the transverse form factors. In the projection on good angular momentum state models, the relevant matrix elements were calculated in the first-order approximation of the expansion of the quantity $\langle J_\perp^2\rangle^{-1} = (\langle\phi_K|2J_y^2|\phi_K\rangle)^{-1}$, where $|\phi_K\rangle$ is an intrinsic axial symmetric state. The final expressions are given by Eqs. (3.27) and (3.31) of Ref. [6].

In the cranking model, we obtain a similar expansion for the form factors in powers of $\mathcal{J}_{\rm cr}^{-1}$, with $\mathcal{J}_{\rm cr}$ being the cranking moment of inertia. We followed here the prescription of Ref. [14] to get the corresponding matrix elements and obtain, for an odd-even system,

$$\begin{aligned}\frac{\langle I_fK\|T^{M\lambda}\|KK\rangle}{\hat{K}} = {} & (KK\lambda0|I_fK)\Bigg[\langle\phi_K|T_0^{M\lambda}|\phi_K\rangle + \frac{I_f(I_f+1)-K(K+1)-\lambda(\lambda+1)}{2\mathcal{J}_{\rm cr}[\lambda(\lambda+1)]^{1/2}} \\ & \times(\langle\phi_K|T_1^{M\lambda}\tilde{\mathcal{E}}_-|\phi_K\rangle - \langle\phi_K|T_{-1}^{M\lambda}\tilde{\mathcal{E}}_+|\phi_K\rangle) \\ & - \frac{[\lambda(\lambda+1)]^{1/2}}{2\mathcal{J}_{\rm cr}}(\langle\phi_K|T_1^{M\lambda}\tilde{\mathcal{E}}_-|\phi_K\rangle + \langle\phi_K|T_{-1}^{M\lambda}\tilde{\mathcal{E}}_+|\phi_K\rangle)\Bigg] \\ & + (K-K\lambda2K|I_fK)\Bigg[\langle\phi_K|T_{2K}^{M\lambda}|\phi_{\bar{K}}\rangle + \frac{[\lambda(\lambda+1)-2K(2K-1)]^{1/2}}{2\mathcal{J}_{\rm cr}} \\ & \times(\langle\phi_K|T_{2K+1}^{M\lambda}\tilde{\mathcal{E}}_+^t|\phi_K\rangle + \langle\phi_K|T_{2K-1}^{M\lambda}\tilde{\mathcal{E}}_-^t|\phi_K\rangle)\Bigg] , \end{aligned} \tag{1a}$$

$$\begin{aligned}\frac{\langle I_fK\|T^{E\lambda}\|KK\rangle}{\hat{K}} = {} & (KK\lambda0|I_fK)\frac{I_f(I_f+1)-K(K+1)}{2\mathcal{J}_{\rm cr}[\lambda(\lambda+1)]^{1/2}}(\langle\phi_K|T_1^{E\lambda}\tilde{\mathcal{E}}_-|\phi_K\rangle + \langle\phi_K|T_{-1}^{E\lambda}\tilde{\mathcal{E}}_+|\phi_K\rangle) \\ & + (K-K\lambda2K|I_fK)\Bigg[\langle\phi_K|T_{2K}^{E\lambda}|\phi_{\bar{K}}\rangle + \frac{[\lambda(\lambda+1)-2K(2K-1)]^{1/2}}{2\mathcal{J}_{\rm cr}} \\ & \times(\langle\phi_K|T_{2K+1}^{E\lambda}\tilde{\mathcal{E}}_+^t|\phi_K\rangle + \langle\phi_K|T_{2K-1}^{E\lambda}\mathcal{E}_-^t|\phi_K\rangle)\Bigg] . \end{aligned} \tag{1b}$$

In the above expressions, we define the operators

$$\tilde{\mathcal{E}}_\pm = \sum_{K'}\frac{|\phi_{K'}\rangle\langle\phi_{K'}|}{\mathcal{E}_{K'}-\mathcal{E}_K}J_\pm , \quad \tilde{\mathcal{E}}_\pm^t = \sum_{K'}\frac{|\phi_{\bar{K}'}\rangle\langle\phi_{K'}|}{\mathcal{E}_{K'}-\mathcal{E}_K}J_\pm ,$$

where $\mathcal{E}_{K'}$ and $\mathcal{E}_K$ are the eigenvalues for the intrinsic Hamiltonian. The electromagnetic operators $T_\nu^{\sigma\lambda}$, with $\sigma = M$ or E, are defined as in Ref. [15], and $\hat{K} = (2K+1)^{1/2}$.

Assuming that the deformed potential which generates the intrinsic wave function is time-reversal invariant, it is possible to recognize in the above expressions, as in the projection model [3,6], zeroth-order terms which are responsible for the contribution from the odd nucleon to the matrix element, first-order terms which receive contributions from all nucleons of the system (the collective terms), and first-order terms which give in general small corrections to the contribution of the odd nucleon. If $\lambda < 2K$, only the first term in Eq. (1b) is different from zero, yielding the collective contribution [6] to the transverse electric form factor of order λ, thus justifying our assertion in the Introduction that the collective contribution can become more evident in inelastic scattering.

Finally, for the particle-rotor model, the matrix elements are [6]

$$\frac{\langle I_f K \| T^{M\lambda} \| KK \rangle}{\hat{K}} = \frac{\langle I_f K \| T^{M\lambda} \| KK \rangle_{\rm sp}}{\hat{K}} + \left[(KK\lambda 0|I_f K) \frac{I_f(I_f+1) - K(K+1) - \lambda(\lambda+1)}{[\lambda(\lambda+1)]^{1/2}} \right.$$
$$\left. - (K\, -K\lambda 2K|I_f K)\langle \chi_K | j_+ | \chi_{\bar{K}} \rangle \delta_{K,1/2} \right] F^{M\lambda} , \tag{2a}$$

$$\frac{\langle I_f K \| T^{E\lambda} \| KK \rangle}{\hat{K}} = \frac{\langle I_f K \| T^{E\lambda} \| KK \rangle_{\rm sp}}{\hat{K}} + \left[(KK\lambda 0|I_f K) \frac{I_f(I_f+1) - K(K+1)}{[\lambda(\lambda+1)]^{1/2}} \right.$$
$$\left. - (K\, -K\lambda 2K|I_f K)\langle \chi_K | j_+ | \chi_{\bar{K}} \rangle \delta_{K,1/2} [\lambda(\lambda+1)]^{1/2} \right] F^{E\lambda} , \tag{2b}$$

with

$$\frac{\langle I_f K \| T^{\sigma\lambda} \| KK \rangle_{\rm sp}}{\hat{K}} = (KK\lambda 0|I_f K)\langle \chi_K | T_0^{\sigma\lambda} | \chi_K \rangle \delta_{\sigma,M} + (K\, -K\lambda 2K|I_f K)\langle \chi_K | T_{2K}^{\sigma\lambda} | \chi_{\bar{K}} \rangle , \tag{3}$$

where $|\chi_K\rangle$ is the wave function for the odd nucleon. The expressions for $F^{\sigma\lambda}$ will depend on rigid rotation or an irrotational-flow assumption (or other prescription) for the core. For the rigid-rotor case, we used Eqs. (5.22) and (5.23) of Ref. [6]. For the irrotational-flow case, we obtain for a general charge distribution, expanded in multipoles [16,17],

$$F_{\rm IF}^{M\lambda} = \frac{i^{\lambda+1}(2\lambda+1)}{(16\pi)^{1/2}\mathcal{J}_{\rm irr}} \sum_{\lambda_1,\lambda_2} \beta_{\lambda_2} R_0^{(2-\lambda_2)} (2\lambda_2+1)[(\lambda_2+1)(2\lambda_2-1)(2\lambda_1+1)]^{1/2}$$
$$\times \begin{pmatrix} \lambda_2-1 & \lambda_1 & \lambda \\ 0 & 0 & 0 \end{pmatrix} \begin{pmatrix} \lambda_1 & \lambda_2 & \lambda \\ 0 & -1 & 1 \end{pmatrix} \begin{Bmatrix} \lambda & \lambda_2-1 & \lambda_1 \\ \lambda_2 & \lambda & 1 \end{Bmatrix} \int r^2 dr\, \rho_{\lambda_1}(r) r^{(\lambda_2-1)} j_\lambda(qr) , \tag{4a}$$

$$F_{\rm IF}^{E\lambda} = i^\lambda \beta_\lambda R_0^{(2-\lambda)} (\lambda+1) \frac{1}{(4\pi)^{1/2} 2\mathcal{J}_{\rm irr}} \int r^2 dr\, r^{\lambda-1} \rho_0(r) j_{\lambda-1}(qr) , \tag{4b}$$

where R_0 is the radius of the equivalent sphere, β_λ is the nuclear deformation parameter of order λ, q is the momentum transferred by the electron, and $\rho_\lambda(r)$ is the charge multipole.

When Coriolis coupling is included in the particle-rotor model, not only will the single-particle matrix element [Eq. (3)] change, but also the collective terms will be different. For the latter, however, this correction will be a second-order effect. As we have considered here terms up to first order in the inverse mass parameter of the system, we included the Coriolis coupling in first order only to the single-particle matrix elements. This modifies Eq. (3) to a form identical to expressions (1a) and (1b) with the only difference that the A particle wave function $|\phi_K\rangle$ is replaced by the odd-nucleon wave function $|\chi_K\rangle$. For the results presented here, numerical calculations have shown that the Coriolis correction in the particle-rotor model makes a significant contribution only for $M\lambda$ multipoles and for the irrotational-flow case.

IV. DISCUSSION OF THE RESULTS

To apply the theoretical results summarized above to the three first states of the ground-state rotational band of ^{25}Mg, the Nilsson model was used to generate the intrinsic structure (pairing correlations were neglected). For the projection and cranking models, the state $|\phi_K\rangle$ for the A nucleon system was built from each individual particle; that is, the inert core assumption was avoided. The magnetization part of the current operator was included in these calculations [15], and the usual center-of-mass and nucleon form-factor corrections were also taken into account. Within the particle-rotor model, the multipole densities $\rho_\lambda(r)$ were obtained from these same individual wave functions. To achieve this, the Nilsson Hamiltonian was diagonalized in a spherical basis where the admixtures of $N = N' \pm 2$ (N being the principal quantum number) were explicitly included. The spin-orbit and L^2 parameters used were the same as those from Ref. [1],

TABLE II. ^{25}Mg values for the deformation parameter δ, the expansion parameter $\langle J_1^2 \rangle$, moments of inertia $\mathcal{I}$, and the ground-state magnetic dipole moment (μ) and dipole transition probability $B(M1)$ to the state at 1.61 MeV.

	Experimental	Theoretical			
δ		0.327			
$\langle J_1^2 \rangle$		18.5			
		PM	CM	RR	IF
$\mathcal{I}$ (M fm^2)	90.0		117.0	160.4	22.0
μ (μ_N)	-0.855^{a}	-1.075	-0.988	-1.062	-1.321
$B[M1;\frac{5}{2}^+ \rightarrow \frac{7}{2}^+]$ (e^2fm^2)	$(7.9\pm1.6)\times10^{-3\,b}$	9.3×10^{-3}	1.1×10^{-2}	7.0×10^{-3}	5.4×10^{-3}

[a] Reference. [7].
[b] Reference [1].

and the deformation parameter δ was chosen to reproduce the experimental electric quadrupole moment of the ground state. It is worthwhile to note that this last quantity has essentially the same value in all rotational models used here, since the intrinsic structure is the same and first-order corrections yield negligible modifications for the quadrupole moment.

Initially, we evaluate the magnetic dipole moment of the ground state and $M1$ transition probability for the first excited state of the band. As is well known, these quantities are equivalent to the magnetic form factor in the low-q limit [15]. The results, within other related quantities such as the deformation parameter, $\langle J_1^2 \rangle$, and moments of inertia, are shown in Table II, where PM

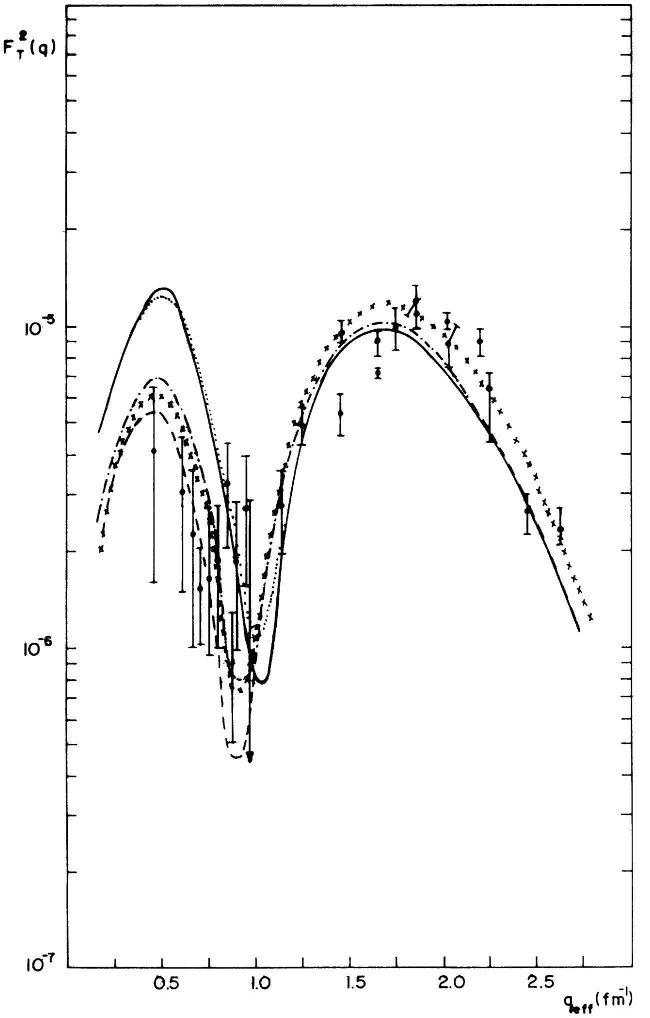

FIG. 2. Transverse elastic form factor for ^{25}Mg, using the Nilsson model without the collective contributions (solid curves) and with collective contributions in the approximations PM (×), CM (dashed curve), RR (dot-dashed curve), and IF (dotted curve). The experimental data are from Refs. [7] and [18].

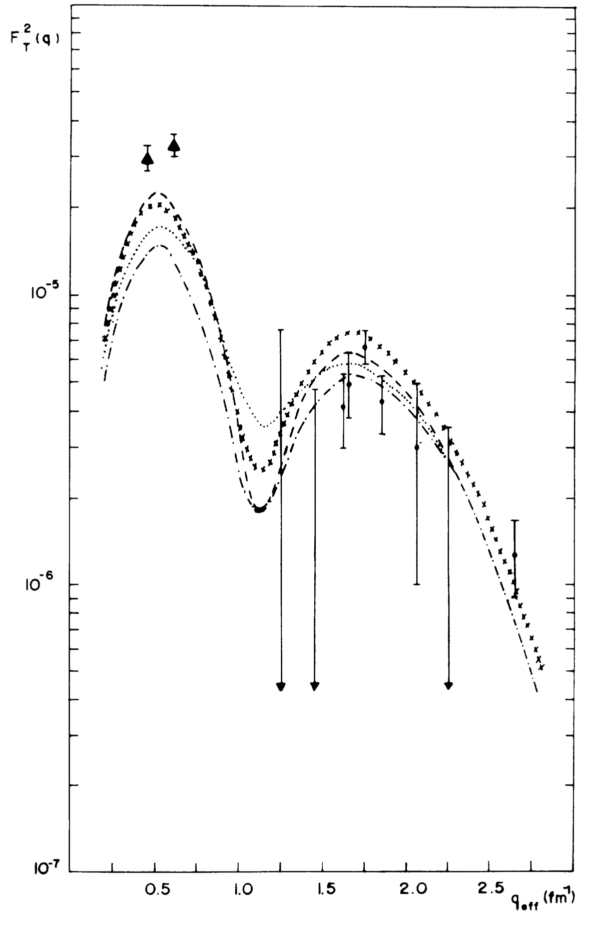

FIG. 3. Transverse form factor for the transition $\frac{5}{2}^+ \rightarrow \frac{7}{2}^+$ (1.612 MeV). Data shown by triangles are from Ref. [19]; data shown by circles are from this work. The conventions for the theoretical form factors are the same as in Fig. 2.

means projection model, CM is cranking model, and RR and IF are the rigid-rotor and irrotational-flow assumptions, respectively, in the framework of the particle-rotor model.

The form factors were calculated in the PWBA, but the experimental points are plotted as a function of an effective momentum transfer (q_{eff}) according to the prescription of Ref. [7]. Figure 2 shows results for the elastic transverse form factors of ^{25}Mg, where the calculation with only the contribution of the odd nucleon in the Nilsson potential, that is, neglecting first-order terms in $\langle J_1^2 \rangle^{-1}$ or $\mathcal{I}^{-1}$, is also shown. As already pointed out [3,4], these are only important in the region of low-q values ($q \leq 1$ fm^{-1}), where the form factor is dominated by the $M1$ multipole. It is also useful to add that, in this low-q region, large differences do exist between the rigid-rotor and irrotational-flow assumptions, the latter yielding results very much the same as those obtained without first-order corrections. As a matter of fact, the core contributions in these two cases yield results very similar for low-q values. However, the Coriolis correlations for irrotational flow are much bigger than for the rigid rotor, as expected, and approximately cancel out the core contributions for the $M1$ multipole in the first case. For the $M3$ multipole the Coriolis correction in the IF case is also important, although it is not seen in the comparison with the data because of the smallness of the total $M3$ form factor (which is true for all models). In the range $q \geq 1$ fm^{-1}, the elastic form factor is dominated by the $M5$ multipole. Except for a small q-independent correction in the PM [6], it depends almost solely on the unpaired nucleon.

In Fig. 3 we can see the form factor for the transition $\frac{5}{2}^+ \rightarrow \frac{7}{2}^+$. In this case, at low-$q$ values, we can see a quite different relation between the form factors calculated in each model. Such differences are explained by the appearance of the $E2$ multipole for this transition. Since our data do not cover this q region, we used old data obtained at 180° [19]. To see even better the $E2$ behavior for the four different theoretical approaches, it is useful to observe Fig. 4, for the transition $\frac{5}{2}^+ \rightarrow \frac{9}{2}^+$. Here the form factor is completely dominated by the $E2$ multipole

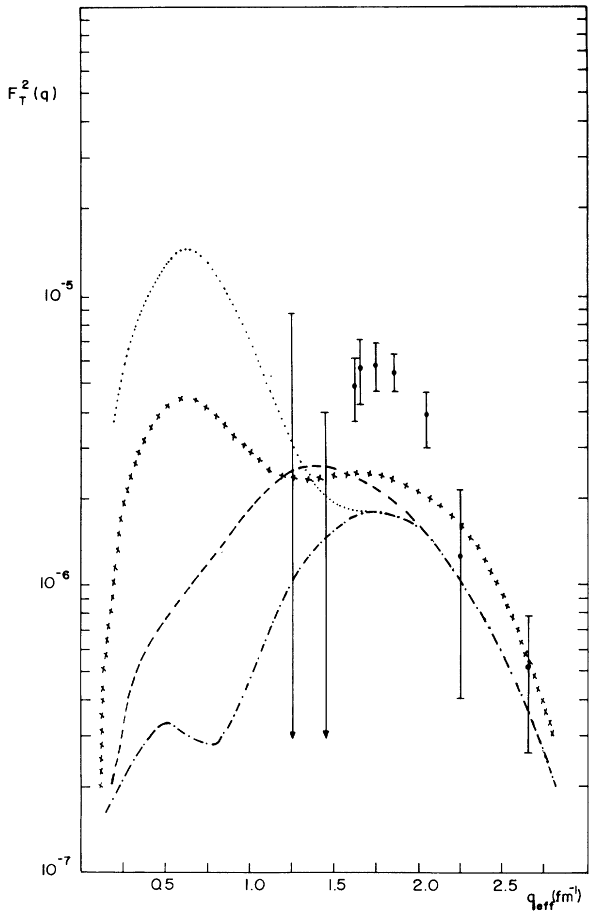

FIG. 4. Transverse form factor for the transition $\frac{5}{2}^+ \rightarrow \frac{9}{2}^+$ (3.405 MeV). The conventions for the theoretical form factors are the same as in Fig. 2, and data points are from this work.

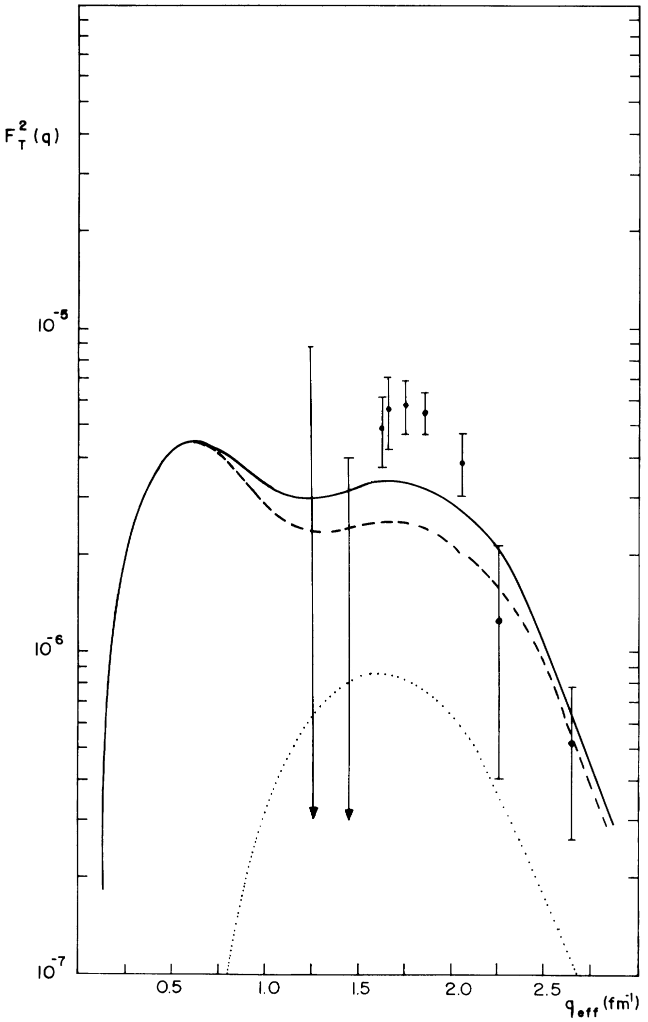

FIG. 5. Transverse form factor for the transition $\frac{5}{2}^+ \rightarrow \frac{3}{2}^-$ (3.413 MeV) calculated in the Nilsson model (dotted curve), for the transition $\frac{5}{2}^+ \rightarrow \frac{7}{2}^+$ (3.405 MeV) calculated in the PM approximation (dashed curve), and the total form factor for these two transitions (solid curve). Data points are the same as in Fig. 4.

for low q (≤ 1 fm^{-1}) and is strongly model dependent. Unfortunately, experimental results are not available at $q \leq 1.2$ fm^{-1} for this transition. For $q \geq 1$ fm^{-1} our calculations show that the form factor is again dominated by the $M5$, with a relatively important contribution of the $M3$ for q between 1.0 and 1.5 fm^{-1}. Other possible multipoles ($E4,E6,M7$) were evaluated and provided negligible contributions. On the other hand, our experimental results are systematically larger than the theoretical ones for most of the covered q region for this transition.

Before criticizing the models for this disagreement, it is worthwhile to note the presence of a $\frac{3}{2}^-$ level at 3.413 MeV on ^{25}Mg, which, because of the experimental resolution, is mixed with the form factor at 3.405 MeV ($\frac{9}{2}^+$). Such a level can be interpreted, in a first approximation, as a member of the rotational band $K^\pi = \frac{1}{2}^-$, which can be explained by a particle excitation in the Nilsson model without changing the nuclear deformation [1]. Under this assumption we estimated the expected form factor for this transition (which includes the multipoles $M2$, $E3$, and $M4$) with the help of the following expression:

$$F^{\sigma\lambda}(q) = \frac{(4\pi)^{1/2}}{Z}\{(K_i K_i \lambda (K_f - K_i)|I_f K_f)\langle \chi_{K_f}|T_\nu^{\sigma\lambda}|\chi_{K_i}\rangle + (K_i - K_i \lambda (K_f + K_i)|I_f K_f) \times \langle \chi_{K_f}|T_\nu^{\sigma\lambda}|\chi_{\bar{K}_i}\rangle\}\ , \tag{5}$$

which corresponds to an interband transition, provided the core effects are ignored.

Figure 5 shows the form factor for the transition $\frac{5}{2}^+ \rightarrow \frac{3}{2}^-$, as well as the addition of this form factor with the one from the $\frac{5}{2}^+ \rightarrow \frac{9}{2}^+$ transition in the PM approach. The discrepancies, which were as large as a factor of 2, are now reduced to at most 30%.

V. CONCLUSIONS

The new experimental data presented in this work demonstrate that the transverse form factors of the first three levels of the ^{25}Mg ground-state rotational band show a systematic behavior very similar to the corresponding results from ^{181}Ta, for which measured transverse form factors were interpreted within the framework of rotational models [4,16]. Unfortunately, however, the strong model dependence in the low-q region for the transition $KK \rightarrow KK+2$ could not be tested for ^{25}Mg. As was already pointed out [6,16], in this case and for $K \geq \frac{3}{2}$, the transverse form factor can bring clear information about the collective convection current in deformed nuclei. This is so, since the magnetization current is negligible for low q [15,17] and the differences between the prediced form factors, on the basis of the rotational models considered here, are as large as the ones observed in even-even nuclei [4,20].

On the other hand, the collective contributions to the $M1$ multipole for ^{25}Mg, for elastic and inelastic scattering, are relatively larger when compared with deformed heavy nuclei. This evidence, independent of the quality of the theoretical results compared with the experiment, can raise the question about the usefulness of the first-order approximation in the *S-D* shell. For ^{25}Mg and at least for the $M1$ multipole, an explicit calculation was made [17] using the exact projection method (all orders in $\langle J_\perp^2 \rangle^{-1}$ were included) and compared with the first-order calculation. At the first peak region, the differences are lower than 10%. These results, combined with other recent calculations for transverse elastic scattering on ^{29}Si [21] and transverse inelastic on ^{24}Mg [20], demonstrate the capability of deformed *S-D* shell nuclei as a potential source of information for the rotational collective currents and to the understanding of its coupling with the single-particle currents.

Finally, we can conclude that for the presently available data for ^{25}Mg, in the region dominated by the $M1$ form factor, the inclusion of the Coriolis coupling to first order in the particle-rotor model clearly discriminates the irrotational-flow assumption, as we can see from the elastic scattering results. We can also conclude that the projection and cranking models appear to work a little better than their phenomenological counterparts, if we look for the first inelastic transition. However, as already stated, a final answer to this question can be given by the measurement of the low-q form factors from the second level of the band.

ACKNOWLEDGMENTS

We acknowledge the cooperation of Dr. W. C. Barber and Dr. S. Kowalski from the MIT Bates Linear Accelerator and Dr. G. A. Peterson from the University of Massachusetts, who helped on the data acquisition, data analysis, and with useful discussions. One of us (J. R. Marinelli) would like to acknowledge CAPES (Coordenadoria de Aperfeiçoamento de Pessoal de Ensino Superior) for partial financial support during the preparation of this paper.

---

[1] E. W. Lees *et al.*, J. Phys. G **2**, 341 (1976).
[2] J. R. Marinelli, MsC. thesis, Universidade de São Paulo, 1980.
[3] E. M. Guerra and A. E. L. Dieperink, Phys. Rev. C **18**, 1596 (1978).
[4] E. M. Guerra, in *Proceedings of the Conference on the Theory of Nuclear Structure and Reactions,* edited by M. Lozano and G. Madurga (World Scientific, Singapore, 1985), p. 329.
[5] T. W. Donnelly and I. Sick, Rev. Mod. Phys. **56**, 461 (1984).
[6] E. M. Guerra, Phys. Rep. **138**, 293 (1986).
[7] H. Euteneuer *et al.*, Phys. Rev. C **16**, 1703 (1977).
[8] W. Bertozzi *et al.*, Nucl. Instrum. Methods **141**, 457 (1977).
[9] S. Kowalski *et al.*, in *Medium Energy Nuclear Physics with Electron Linear Accelerators—MIT 1967 Summer Study,* U.S. Atomic Energy Commission Technical Infor-

mation Division, Report No. T10-24667, edited by W. Bertozzi and S. Kowalski, p. 39.

[10] W. Bertozzi *et al.*, Nucl. Instrum. Methods **162**, 211 (1979).

[11] J. Bergstrom *et al.*, in *Medium Energy Nuclear Physics with Electron Linear Accelerators—MIT 1967 Summer Study*, U.S. Atomic Energy Commission Technical Information Division, Report No. T10-24667, edited by W. Bertozzi and S. Kowalski, p. 251.

[12] T. Cooper *et al.*, Phys. Rev. C **13**, 1083 (1976).

[13] Y. Okazaki *et al.*, Research Report of Laboratory of Nuclear Science, Tohoku University, Vol. 7, No. 1, 43 (1974).

[14] M. Radomski, Phys. Rev. C **14**, 1704 (1976).

[15] T. de Forest and J. D. Wallecka, Adv. Phys. **15**, 1 (1966).

[16] M. Nishimura, D. W. L. Sprung, and E. M. Guerra, Phys. Lett. **161B**, 235 (1985).

[17] J. R. Marinelli, Ph.D. thesis, Universidade de São Paulo, 1988.

[18] R. C. York and G. A. Peterson, Phys. Rev. C **19**, 574 (1979).

[19] L. W. Fagg *et al.*, Phys. Rev. **187**, 1384 (1969).

[20] J. R. Marinelli and J. R. Moreira, Phys. Rev. C **39**, 1242 (1989).

[21] E. Graça *et al.*, Nucl. Phys. **A483**, 77 (1988).